Excitation of Mach cones and energy dissipation by charged particles moving over two-dimensional strongly coupled dusty plasmas

Ke Jiang, Lu-Jing Hou, and You-Nian Wang*
State Key Lab of Materials Modification by Beams, Department of Physics,Dalian University of Technology, Dalian, China 116023

Z. L. Mišković
Department of Applied Mathematics, University of Waterloo, Waterloo, Ontario, Canada N2L 3G1
(Received 4 August 2005; published 20 January 2006)

We present a theoretical model for studying the interactions of charged particles with two-dimensional strongly coupled dusty plasmas, based on the quasilocalized charge approximation in which the static pair distribution function of a dust layer is determined from a molecular dynamics simulation. General expressions are derived for the perturbed dust-layer density, the induced potential in plasma, and the energy loss of a charged particle moving parallel to the dust layer. Numerical results show that the structure of Mach cones, excited in the dust layer by the charged particle, strongly depends on the plasma parameters such as the coupling parameter, the screening parameter, and the discharge pressure, as well as on the particle speed. In addition, it is found that the energy dissipation suffered by slow charged particles can be significantly enhanced in strongly coupled dusty plasmas when compared to the dissipation in weakly coupled plasmas.

DOI: 10.1103/PhysRevE.73.016404 PACS number(s): 52.40.Hf, 52.25.Vy, 52.35.Fp

I. INTRODUCTION

A dusty, or complex, plasma is an ionized gas in which submicron-to-micron sized particles, usually called dust grains, are embedded [1–5]. Dusty plasmas occur widely in astrophysical environments, as well as in the laboratory settings where they allow direct optical imaging of particle motion in real time. Typically, dust particles in the laboratory plasmas acquire large negative charges, of the order of $Z_d \sim 10^3$ to 10^4 elementary charges, so that they can interact quite strongly with each other via the screened Coulomb (Yukawa) potential $\phi(r)=[(Z_d e)^2/r]\exp(-r/\lambda_D)$, where r is the interparticle distance, e is electron charge, and λ_D is the Debye screening length of the background plasma. Dust particles usually form two-dimensional (2D) layers in the laboratory plasmas, which can be classified by means of two parameters. One is the lattice parameter, or interaction range, $\kappa=a/\lambda_D$, where $a=(\pi\sigma_{d0})^{-1/2}$ is the average interparticle distance with σ_{d0} being the equilibrium surface density of the dust layer. The other parameter is the Coulomb coupling Γ, defined as the ratio of the interparticle interaction energy to the particle thermal kinetic energy, $\Gamma=(Z_d e)^2/(aT_d)$, where T_d is the dust layer temperature (in units of energy). When $\Gamma \gg 1$, the dust system is said to be strongly coupled and, consequently, the particles tend to arrange themselves into liquidlike or crystalline structures, as shown in the microphotographs reported in Refs. [2–5].

Ever since strongly coupled dusty plasmas were first created in 1994, the wave phenomena in these structures have been extensively studied, both theoretically [6,7] and experimentally [8,9]. Two wave modes have been identified in 2D dust crystals: a longitudinal (compressional) wave in which particles are displaced parallel to the direction of the wave vector **k**, and a transverse (shear) wave in which particles are displaced perpendicular to **k**. A comprehensive theory of both types of waves in Yukawa crystals has been recently developed by Wang *et al.* [10] and subsequently verified in considerable detail in the experiments conducted by Nunomura *et al.* [11]. Dusty plasmas in the gaseous (weakly coupled) state can sustain compressional waves but not transverse waves. The most ubiquitous are the dust acoustic waves (DAW) [12,13] which have low frequency due to the large mass of dust grains. In the liquid phase, strong coupling is expected to soften the longitudinal dispersion and to generate a transverse (shear) mode, in qualitative resemblance to the phonon spectrum of a lattice [14].

The existence of Mach-cone waves in complex plasmas was first predicted by Havnes *et al.* [15], who described how a charged body moving through a cloud of dust particles can excite a DAW. Their report initiated a series of experimental [16–19], as well as theoretical analytical [20–24] and simu-

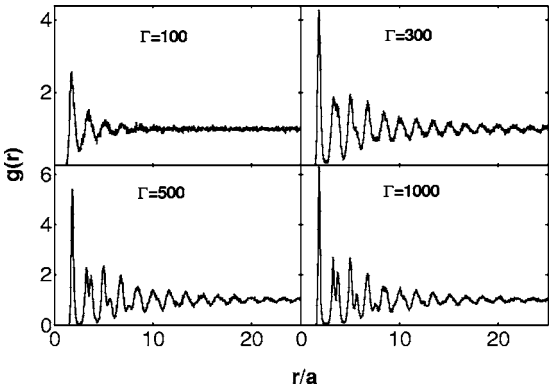

FIG. 1. Pair correlation functions of dust layer in equilibrium with $\kappa=1$ and for $\Gamma=100$, 300, 500, and 1000.

*Email address: ynwang@dlut.edu.cn

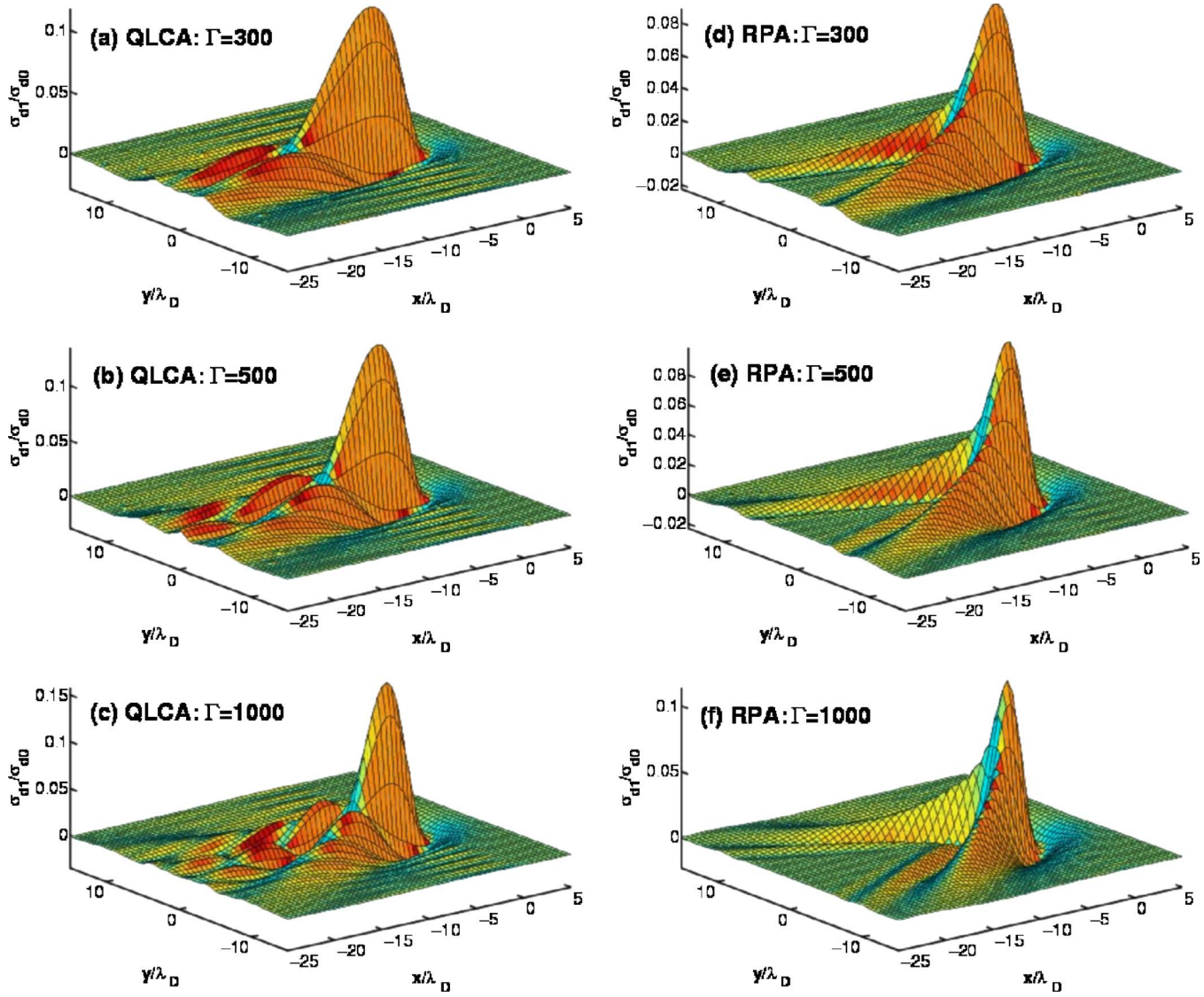

FIG. 2. (Color online) Perturbed density σ_{d1} in the Mach cone region for different coupling constants: $\Gamma=300$ (a) and (d), 500 (b) and (e), and 1000 (c) and (f), based on the QLCA [(a), (b), and (c)] and the RPA [(d), (e), and (f)] descriptions. Here, the screening constant $\kappa=1$, the projectile speed $v=1$ cm/s, and the discharge pressure $p=10$ Pa are kept fixed.

lation [25], studies of this topic. Mach cones can be excited by laser beams [18,19] and by charged particles [16,17]. In particular, Mach cones excited by charged particles were first observed experimentally in the earth laboratories by Samsonov *et al.* [16,17] in a gas discharge experiment. In their experiment, they observed that some V-shaped density disturbances, i.e., Mach cones, were excited in a 2D monolayer dust crystal by Brownian particles moving slightly below the layer. The opening angles of Mach cones, θ, were found to obey the Mach-cone-angle relation, $\sin\theta=v_s/v$, with v_s being the dust acoustic speed and v the speed of the moving particle. This rule was also verified in a wide range of Mach numbers in other experiments. On the theoretical side, analytical theory of Mach cones induced by the motion of charged particles was formulated by Dubin [20], who applied the linear theory of phonon response to a 2D dust crystal, and such an approach provided additional insight in the experimental observations [16,17] for this excitation method.

On the other hand, a charged particle will normally lose its kinetic energy while exciting Mach cones in a dusty plasma. Nasim *et al.* [26] were the first to study, within the linear dielectric response theory, the energy loss of two correlated ions passing through a bulk of a three-dimensional (3D) dusty plasma. Shortly thereafter, this work was extended to include the dust-neutral collisions [27] and the dust-charge fluctuation [28,29]. It should be stressed that these studies were focused mainly on the energy loss of projectile particles moving through homogeneous 3D dusty plasmas, containing weakly correlated dust particles. However, most experiments [15–18] on Mach cones were observed in 2D strongly coupled dusty plasmas, and it is not a straightforward matter to generalize the approach of previous works [26–29] to such systems.

The purpose of this paper is to develop a theoretical model for studying Mach cones excited by a charged particle moving over a 2D strongly coupled dusty plasma. To this end, we use the quasilocalized charge approximation

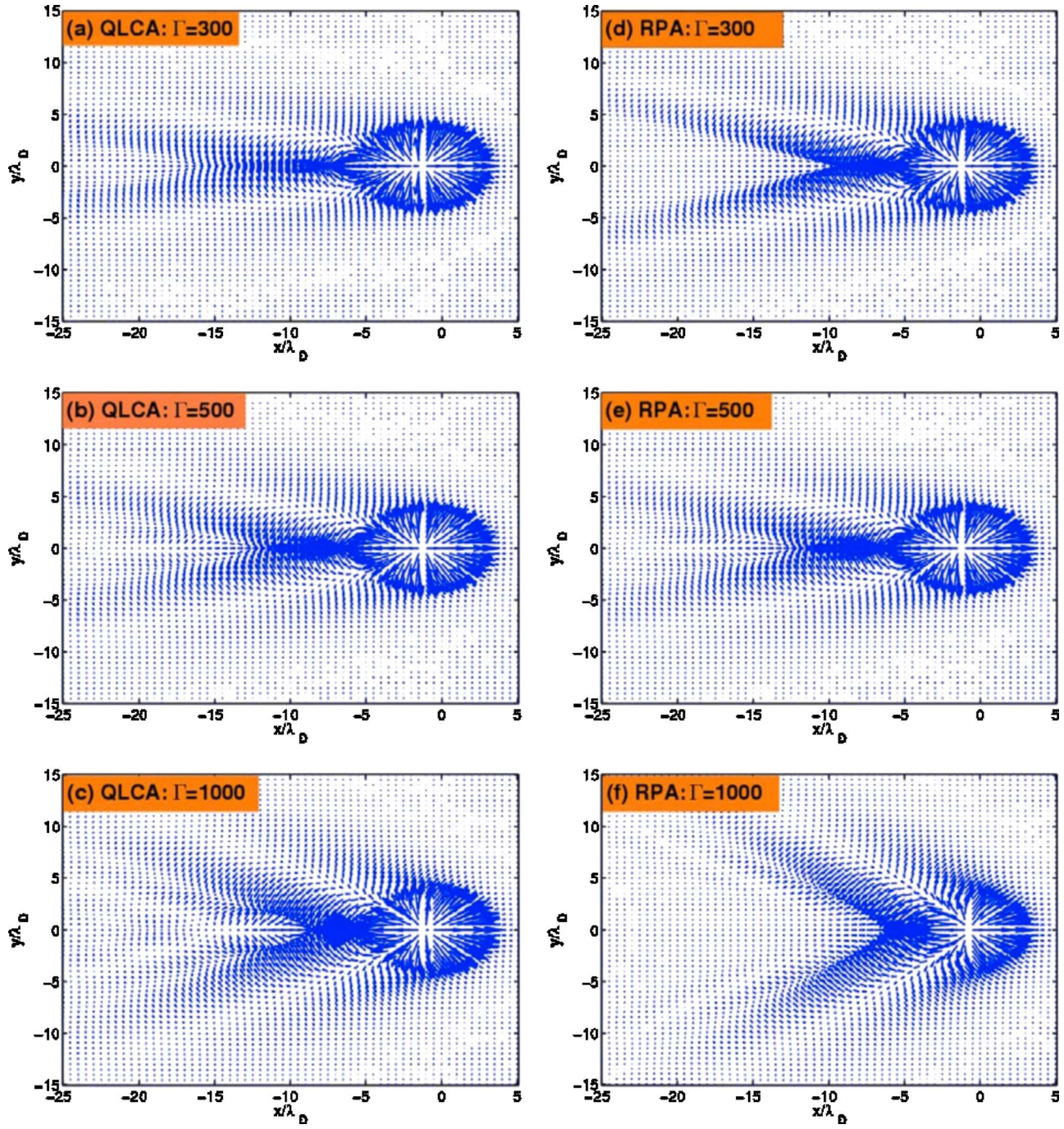

FIG. 3. (Color online) Velocity field $\mathbf{u}_{d1}$ in the Mach cone region for the same parameters as in Fig. 1.

(QLCA) [30–34], which has been successfully used before to study collective excitations in 2D and 3D Yukawa systems. In addition, damping effects due to the collisions of dust particles with neutrals are taken into account in our model by means of a phenomenological factor [35]. The pair correlation function of dust particles, $g(r)$, which is needed in QLCA, is determined here by the molecular dynamics (MD) simulation method. Finally, the energy losses of charged particles are studied in detail for a range of plasma parameters.

The paper is organized as follows. In Sec. II, general expressions are derived on the basis of QLCA for the perturbed density and velocity fields in a 2D dust layer due to a moving external charged particle. Numerical results for these quantities are discussed in Sec. II for different plasma parameters. In Sec. III, we use Poisson equation in conjunction with the perturbed dust-layer density to study the influence of strong coupling on the energy loss of the moving particle. Finally, a short summary is presented in Sec. IV.

II. MACH CONES

Consider a dust layer in the plane $z=0$ of a Cartesian coordinate system with $\mathbf{R}=\{x,y,z\}$, which is immersed in a

large volume of plasma with density n_0. Bulk conditions are reached for such distances from the dust layer that $|z| \gg \lambda_D$, and we assume that the plasma is quasineutral there, $n_{e\infty}=n_{i\infty}=n_0$. The dust layer consists of N_d particles at the equilibrium positions $\mathbf{r}_j=\{x_j,y_j\}$, with $j=1,2,\ldots,N_d$. Let $\sigma_d(\mathbf{r},t)$ and $\mathbf{u}_d(\mathbf{r},t)$ be, respectively, the density and the velocity field (having only the x and y components) of the dust layer at the position $\mathbf{r}=\{x,y\}$ and at time t. The equilibrium density of the layer is given by $\sigma_{d0}=\Sigma_{j=1}^{N_d}\langle\rho(\mathbf{r}_j)\rangle$, where $\rho(\mathbf{r}_j)=\delta(\mathbf{r}-\mathbf{r}_j)$ is the single-particle density and $\langle\ldots\rangle$ is an ensemble average over the dust structure realizations in equilibrium. The particles interact with each other through a screened Coulomb potential $\phi(r_{ij})$.

Now consider a projectile particle with the charge $-Z_te$ and velocity $\mathbf{v}$, moving parallel to the dust layer at the constant height h, which produces an external potential $\Phi_{ext}(\mathbf{r},z,t)=-Z_te\exp(-\eta/\lambda_D)/\eta$, where $\eta \equiv \sqrt{|\mathbf{r}-\mathbf{v}t|^2+(z-h)^2}$. Assuming that Φ_{ext} presents a small disturbance in the dust layer, its density and velocity fields can be expressed as $\sigma_d(\mathbf{r},t)=\sigma_{d0}+\sigma_{d1}(\mathbf{r},t)$ and $\mathbf{u}_d(\mathbf{r},t) \equiv \mathbf{u}_{d1}(\mathbf{r},t)$, where the first-order perturbations of these quantities are respectively given by the ensemble averages,

$$\sigma_{d1}(\mathbf{r},t)=\sum_{j=1}^{N_d}\langle\rho(\mathbf{r}_j+\boldsymbol{\zeta}_j(t))-\rho(\mathbf{r}_j)\rangle, \tag{1}$$

$$\mathbf{u}_{d1}(\mathbf{r},t)=\sum_{j=1}^{N_d}\left\langle\frac{d\boldsymbol{\zeta}_j(t)}{dt}\right\rangle, \tag{2}$$

where $\boldsymbol{\zeta}_j(t)$ is the displacement amplitude of the jth dust particle from its equilibrium position $\mathbf{r}_j$.

In the following, we use the QLCA to determine the single-particle positions $\boldsymbol{\zeta}_j(t)$. The physical picture of the QLCA is that the dust particles are trapped in a local potential where they undergo small oscillations around their equilibrium sites $\mathbf{r}_j$, such that the oscillation amplitudes $|\boldsymbol{\zeta}_j(t)|$ remain much smaller than the interparticle distance a. Following the procedure of Refs. [30–34], we can describe the microscopic motion of a single particle by

$$-\omega^2\boldsymbol{\zeta}_{\mathbf{k}}(\omega)=-\left[\mathbf{D}(\mathbf{k})+\frac{\sigma_{d0}\phi(k)}{m_d}\mathbf{kk}\right]:\boldsymbol{\zeta}_{\mathbf{k}}(\omega)+i\gamma\omega\boldsymbol{\zeta}_{\mathbf{k}}(\omega)+\frac{\sigma_{d0}}{(m_dN_d)^{1/2}}\mathbf{F}_{ext}(\mathbf{k},\omega), \tag{3}$$

where $\mathbf{k}=\{k_x,k_y\}$ and m_d is the dust particle mass, while the collective coordinates $\boldsymbol{\zeta}_{\mathbf{k}}(\omega)$ are defined via the 2D Fourier transform,

$$\boldsymbol{\zeta}_j(t)=\frac{1}{2\pi\sqrt{m_dN_d}}\sum_{\mathbf{k}}\int d\omega\boldsymbol{\zeta}_{\mathbf{k}}(\omega)\exp(i\mathbf{k}\cdot\mathbf{r}_j-i\omega t). \tag{4}$$

In Eq. (3), $\mathbf{D}(\mathbf{k})$ is the 2D QLCA dynamical matrix, which is a functional of the static pair correlation function of the dust layer, $g(\mathbf{r})$, or its Fourier transform $g(\mathbf{k})$, given by [30–34]

$$\mathbf{D}(\mathbf{k})=\frac{1}{V_{2D}}\sum_{\mathbf{q}}\frac{\sigma_{d0}\phi(k)}{m_d}\mathbf{qq}[g(|\mathbf{q}-\mathbf{k}|)-g(\mathbf{q})], \tag{5}$$

with $\phi(k)=2\pi(Z_de)^2/\sqrt{k^2+\lambda_D^{-2}}$ being the 2D Fourier transform of the the potential $\phi(r)$, and V_{2D} the area of the 2D dust layer. The second term on the right-hand side of Eq. (3) comes from the friction force due to the collisions of dust particles with neutral atoms/molecules in the plasma, where the factor γ is the Epstein drag coefficient [31]. The last term in Eq. (3) is related to the external disturbance, with the 2D Fourier transform, $\mathbf{F}_{ext}(\mathbf{k},\omega)$, of the external force $\mathbf{F}_{ext}(\mathbf{r},t)=Z_de\boldsymbol{\nabla}_{\mathbf{r}}\Phi_{ext}(\mathbf{r},z,t)|_{z=h}$ given by

$$\mathbf{F}_{ext}(\mathbf{k},\omega)=i\mathbf{k}\frac{4\pi Z_tZ_de^2}{\sqrt{k^2+\lambda_D^{-2}}}\exp(-h\sqrt{k^2+\lambda_D^{-2}})\,\delta(\omega-\mathbf{k}\cdot\mathbf{v}). \tag{6}$$

It is clear that the dynamical matrix reflects the correlation effects between the dust particles, so that Eq. (3) will be reduced to the well-known result, predicted by the random-phase approximation (RPA) theory, when $\mathbf{D}(\mathbf{k})=0$.

After Fourier transforming the Eqs. (1) and (2), one can use Eq. (3) to write the Fourier transform of the perturbed density and the velocity of the dust layer as follows:

$$\sigma_{d1}(\mathbf{k},\omega)=i\frac{\sigma_{d0}}{m_d}\frac{\mathbf{k}\cdot\mathbf{F}_{ext}(\mathbf{k},\omega)}{H_L(k,\omega)}, \tag{7}$$

$$\mathbf{u}_{d1}(\mathbf{k},\omega)=i\frac{\omega\sigma_{d0}}{m_d}\left(\frac{N_d}{m_d}\right)^{1/2}\left[\frac{\hat{\mathbf{k}}\hat{\mathbf{k}}}{k^2H_L(k,\omega)}+\frac{k^2\hat{\mathbf{I}}-\hat{\mathbf{k}}\hat{\mathbf{k}}}{k^2H_T(k,\omega)}\right]\cdot\mathbf{F}_{ext}(\mathbf{k},\omega), \tag{8}$$

where the auxiliary functions

$$H_L(k,\omega)\equiv\omega(\omega+i\gamma)-\omega_0^2(k)[1+D_L(k)], \tag{9}$$

$$H_T(k,\omega)\equiv\omega(\omega+i\gamma)-\omega_0^2(k)D_T(k), \tag{10}$$

are expressed in terms of the longitudinal and transverse projections of the QLCA dynamical matrix, $D_L(k)$ and $D_T(k)$, defined by

$$D_L(k)=\frac{\omega_{pd}^2\lambda_D^2}{2}\int_0^\infty dr\frac{g(r)-1}{r^2}\exp\left(-\frac{r}{\lambda_D}\right)\left[\left(1+\frac{r}{\lambda_D}+\frac{r^2}{\lambda_D^2}\right)-\left(4+\frac{4r}{\lambda_D}+\frac{2r^2}{\lambda_D^2}\right)J_0(kr)+\left(6+\frac{6r}{\lambda_D}+\frac{2r^2}{\lambda_D^2}\right)\frac{J_1(kr)}{kr}\right], \tag{11}$$

$$D_T(k)=\omega_{pd}^2\lambda_D^2\int_0^\infty dr\frac{g(r)-1}{r^2}\exp\left(-\frac{r}{\lambda_D}\right)[1-J_0(kr)]\times\left(1+\frac{r}{\lambda_D}+\frac{r^2}{\lambda_D^2}\right)-D_L(k). \tag{12}$$

In Eqs. (9) and (10), $\omega_0(k)$ is the frequency of the

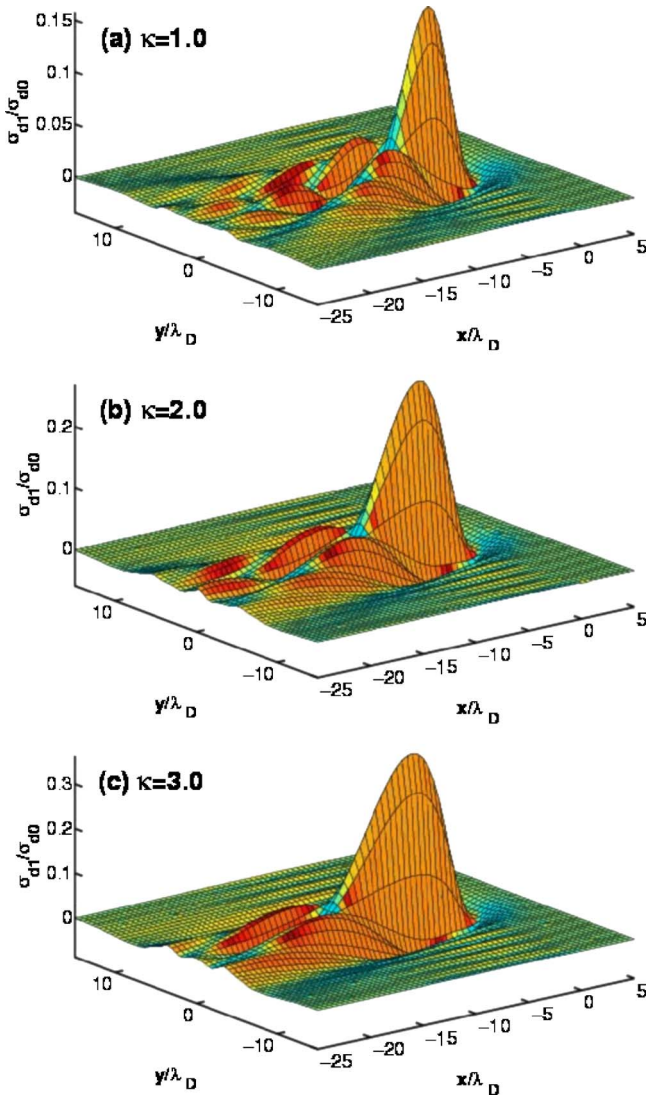

FIG. 4. (Color online) Perturbed density σ_{d1} in the Mach cone region for different screening constants: $\kappa=1$ (a), 2 (b), and 3 (c), based on the QLCA description. Here, the coupling constant $\Gamma=100$, the projectile speed $v=1$ cm/s, and the discharge pressure $p=10$ Pa are kept fixed.

longitudinal-acoustic wave in the RPA description,

$$\omega_0^2(k) = \frac{\omega_{pd}^2 (k\lambda_D)^2}{\sqrt{1+(k\lambda_D)^2}}, \tag{13}$$

with

$$\omega_{pd} = \left(\frac{2\pi e^2 Z_d^2 \sigma_{d0}}{m_d \lambda_D}\right)^{1/2} \tag{14}$$

being the dusty plasma frequency. On using the Eq. (6) in Eqs. (7) and (8), we finally obtain the perturbed density,

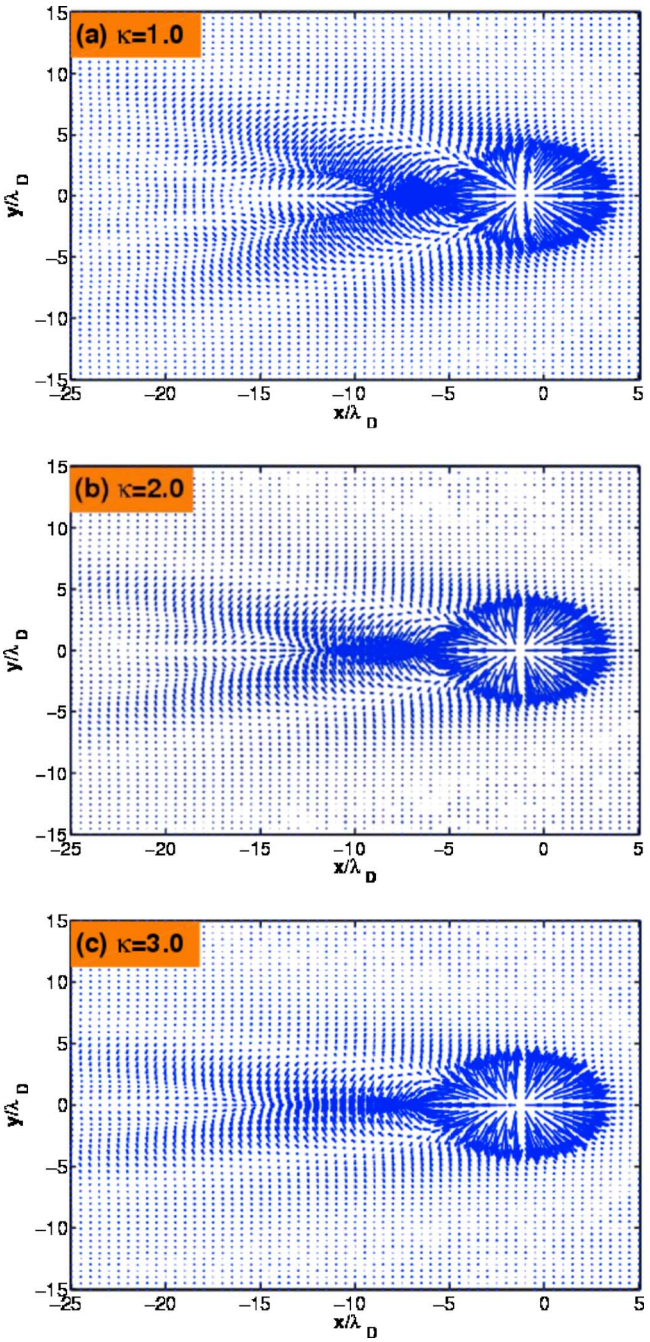

FIG. 5. (Color online) Velocity field $\mathbf{u}_{d1}$ in the Mach cone region for the same parameters as in Fig. 3.

$$\sigma_{d1}(\mathbf{r},t) = \frac{2Z_t e \sigma_{d0}}{m_d} \int \frac{d^2\mathbf{k}}{(2\pi)^2} \frac{(k\lambda_D)^2}{\sqrt{1+(k\lambda_D)^2}} \times \frac{\exp(-h\sqrt{1+(k\lambda_D)^2}/\lambda_D)}{H_L(k,\mathbf{k}\cdot\mathbf{v})} e^{i\mathbf{k}\cdot(\mathbf{r}-\mathbf{v}t)}, \tag{15}$$

whereas the expression for the perturbed velocity $\mathbf{u}_{d1}(\mathbf{r},t)$ follows in analogy to Eq. (15). It is clear from this equation that both the perturbed density and the perturbed velocity are stationary fields in the frame of reference moving at the velocity $\mathbf{v}$ of the projectile particle.

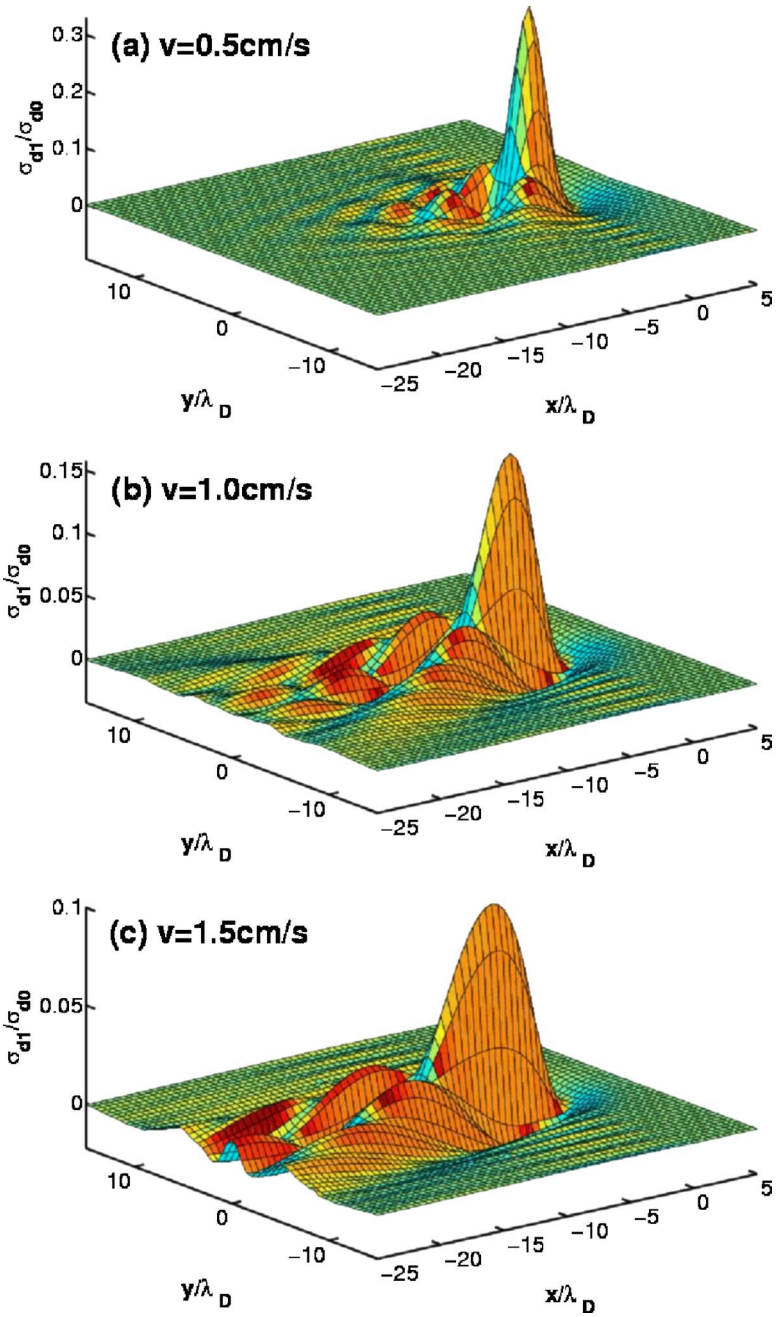

FIG. 6. (Color online) Perturbed density σ_{d1} in the Mach cone region for different projectile speeds: $v=0.5$ cm/s (a), 1 cm/s (b), and 1.5 cm/s (c), based on the QLCA description. Here, the coupling constant $\Gamma=100$, the screening constant $\kappa=1$, and the discharge pressure $p=10$ Pa are kept fixed.

The main parameters used in our numerical computations are all selected in accordance with recent Mach-cone experiments in dusty plasmas [16–19]. The base values of the parameters are as follows. The bulk plasma density, $n_0=1\times10^8$ cm^{-3}; the ion temperature and the dust temperature, $T_i=T_d=0.1$ eV; the electron temperature, $T_e=3$ eV; the mass density and the radius of dust particles, $\rho_d=1.5$ g/cm^3 and $r_d=4.5$ μm (so that $m_d\approx5.7\times10^{-10}$ g). Under these conditions, the Debye length is $\lambda_D\approx231$ μm, and the thermal speeds of electrons, ions, and dust particles are respectively $v_{e,th}\approx7.2\times10^7$ cm/s, $v_{i,th}\approx5\times10^4$ cm/s and $v_{d,th}\approx2\times10^{-3}$ cm/s. The charge on the projectile dust particle is kept fixed at $Z_t=10\,000$, whereas its height above the dust layer is chosen to be $h=2\lambda_D$. Finally, the speed of the projectile particle v, the coupling parameter Γ, the screening parameter κ of the 2D dust layer, and the discharge pressure p (which determines the damping constant γ), are treated as variable parameters. Note that the charge on dust particles Z_d, the surface number density σ_{d0}, and consequently the dusty plasma frequency ω_{pd} and the dust-acoustic speed v_s, all depend on Γ and κ. Typically, when $\Gamma=1000$ and $\kappa=1$, we obtain $Z_d\approx4005$, $\omega_{pd}\approx32$ Hz, and $v_s\approx0.74$ cm/s. We note that the theory works equally well for both the sub- and supersonic projectile speeds.

In addition, we perform a MD simulation with N_d particles to determine the static pair correlation function $g(r)$ to be used in Eq. (5). The simulation consists of two steps. First, we track Brownian motions of $N_d=1600$ charged dust particles which are initially randomly located in a plane with the rectangular periodic boundary conditions and are allowed

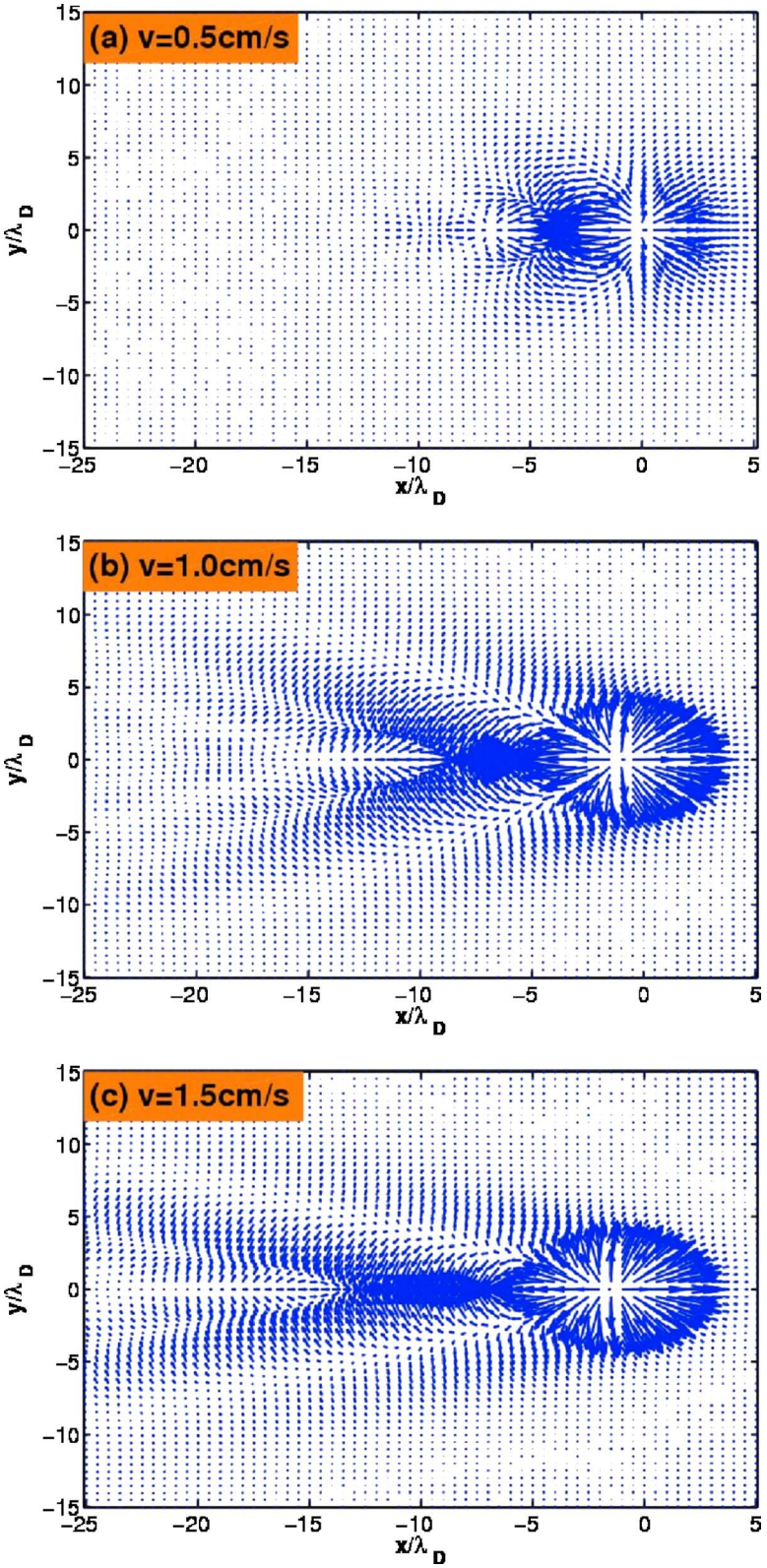

FIG. 7. (Color online) Velocity field $\mathbf{u}_{d1}$ in the Mach cone region for the same parameters as in Fig. 5.

to interact with each other via the screened Coulomb potential $\phi(r)$. The Brownian motions are generated by asymmetric molecular bombardment from the neutral gas, which counteracts the ordering tendency of Coulomb forces, and its intensity is determined by the pressure of the background gas. The strength of the interparticle interactions is fully characterized by the coupling coefficient Γ and the screening parameter κ. Details of such simulation technique are explained in, e.g., Ref. [36]. After running the simulation long enough, the system reaches an equilibrium from which an ensemble-averaged pair correlation function $g(r)$ is calculated. Several examples of this function are shown in Fig. 1

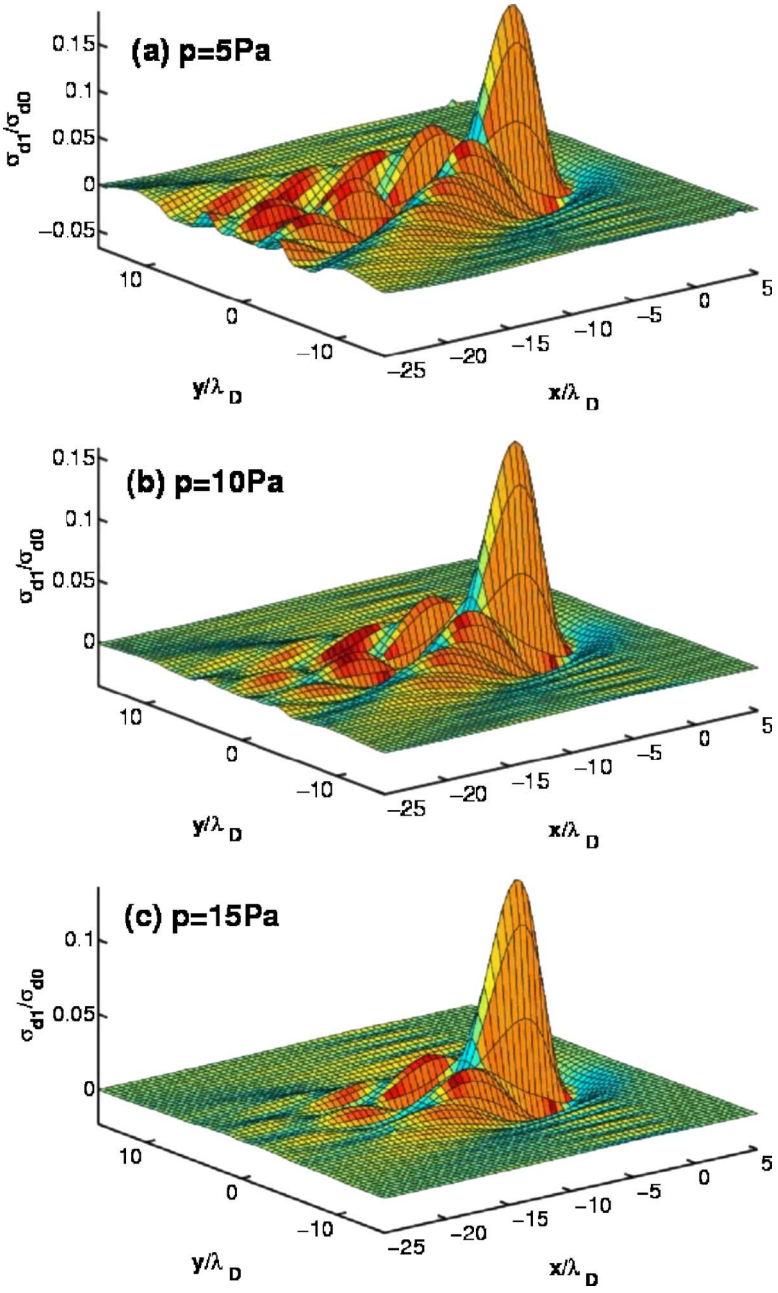

FIG. 8. (Color online) Perturbed density σ_{d1} in the Mach cone region for different discharge pressures: $p=5$ Pa (a), 10 Pa (b), and 15 Pa (c), based on the QLCA description. Here, the coupling constant $\Gamma=100$, the screening constant $\kappa=1$, and the speed $v=1$ cm/s are kept fixed.

with $\kappa=1$ and for $\Gamma=100$, 300, 500, and 1000. It should be noted that, while the original proposers of QLCA suggested that their theory should be reliable for $\Gamma>10$ in systems with bare Coulomb interactions, we limit ourselves here to values $\Gamma>100$ to compensate for reduction in the effective coupling parameter Γ_{eff} in systems with screened Coulomb interactions. In the second step of our simulation, a charged particle is projected horizontally into the system at the velocity $\mathbf{v}$ and at a constant height h over the dust layer. The details of interactions between the projectile particle and all Brownian particles in the layer are recorded and the stopping power of the projectile is calculated directly, providing a measure of energy losses due to the excitations of the collective motion of the dust layer and due to Epstein drag. It should be noted that the velocity of the projectile particle is kept fixed in each simulation run for simplicity. In other words, neither the slowing down of the projectile due to stopping power, nor the competing acceleration processes of the projectile, which were observed in recent experiments [16,17,37], are considered in the present version of our simulation.

We next analyze the dependence of the Mach-cone structure on the coupling parameter Γ of a 2D dust layer. Figure 2 shows the results for the perturbed density σ_{d1} in the Mach-cone region for different coupling constants: $\Gamma=300$, 500, and 1000, with the discharge pressure $p=10$ Pa, the screening parameter $\kappa=1$, and the projectile speed $v=1$ cm/s kept fixed. For comparison, we also show in Fig. 2 the corresponding results produced by the RPA description. One can clearly identify V-shaped Mach cones, along with multiple oscillatory lateral wakes, exhibiting several features. First, it can be seen that

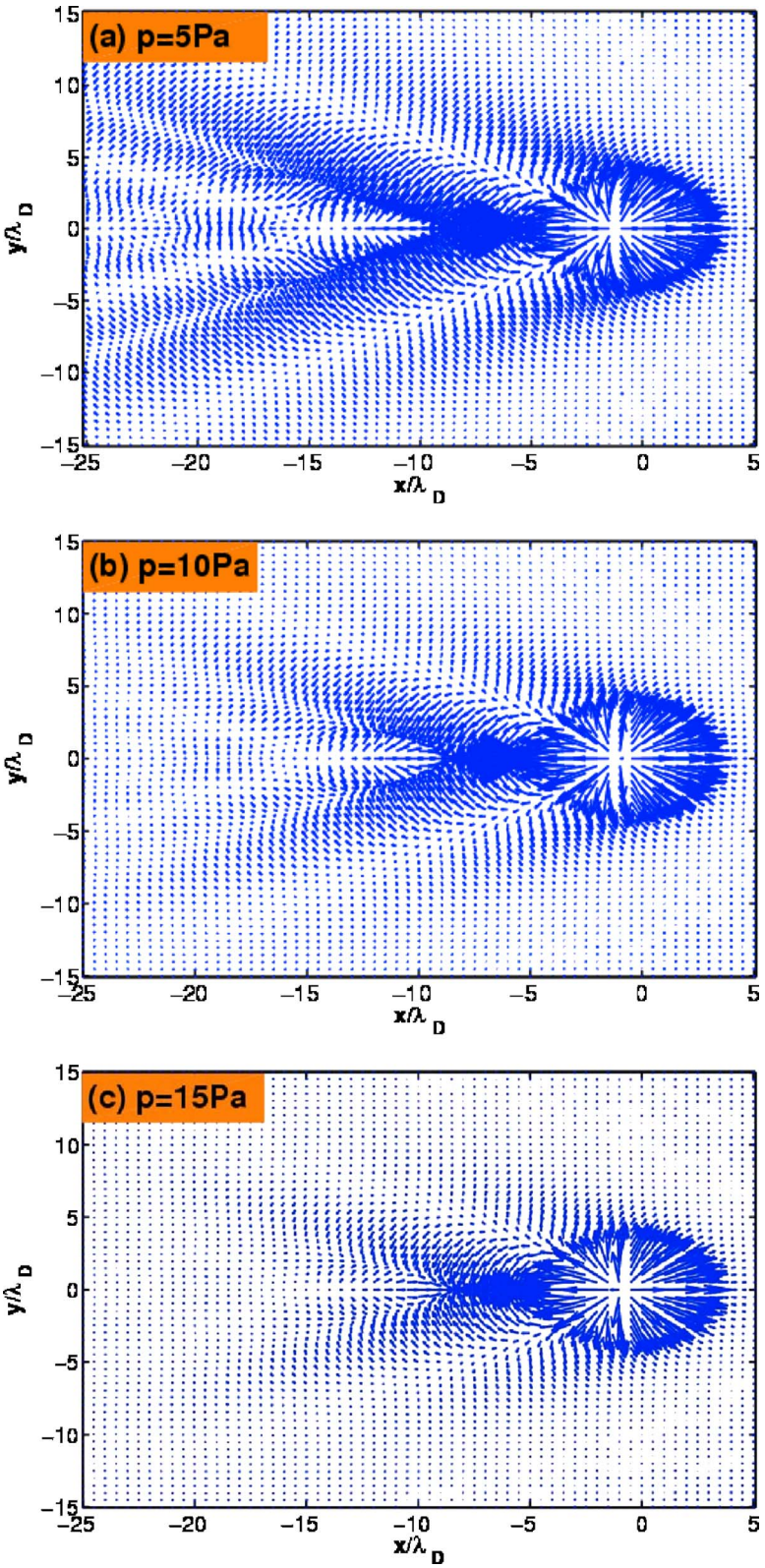

FIG. 9. (Color online) Velocity field $\mathbf{u}_{d1}$ in the Mach cone region for the same parameters as in Fig. 7.

these structures are composed of multiple cones, with the outermost one being the most pronounced, which is a consequence of strongly dispersive nature of the dust-acoustic waves, according to an earlier theory [20] of Mach cones in dusty plasmas. Second, Mach cones in Fig. 2 are composed of the compressional waves, which can be more clearly observed in the maps of the dust velocity field $\mathbf{u}_{d1}$, shown in Fig. 3 for the same parameters as in Fig. 2. In Fig. 3 one can see that the direction of the dust particle motion is perpendicular to the cone wings and parallel to the direction of wave propagation, indicating that the Mach cones are indeed compressional

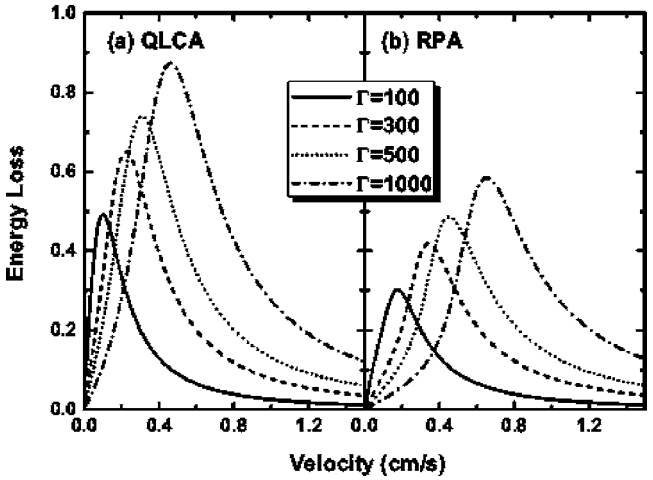

FIG. 10. The normalized energy loss, $S\lambda_D/T_e$, of the projectile charge versus its velocity in a dusty plasma, based on both the QLCA (a) and the RPA (b) descriptions, for different coupling constants: $\Gamma=100$, 300, 500, and 1000. Here, the screening constant $\kappa=1$, the discharge pressure $p=10$ Pa, and the height of the particle $h=2\lambda_D$ are kept fixed.

waves. Furthermore, the cone opening angle is seen in Fig. 3 to increase with Γ, whereas the amplitude of Mach cones in Fig. 2 remains approximately constant. Moreover, one can conclude that both the structures and the amplitudes of Mach cones, given by the QLCA, are quite different from those given by the RPA. In particular, the wings of Mach cones in Fig. 2 are seen to oscillate in the longitudinal direction in the QLCA description, but not in the RPA description, as a result of contributions from the local field function $D_L(k)$.

We consider next the dependence of the Mach-cone structure on the screening parameter κ in the QLCA description.

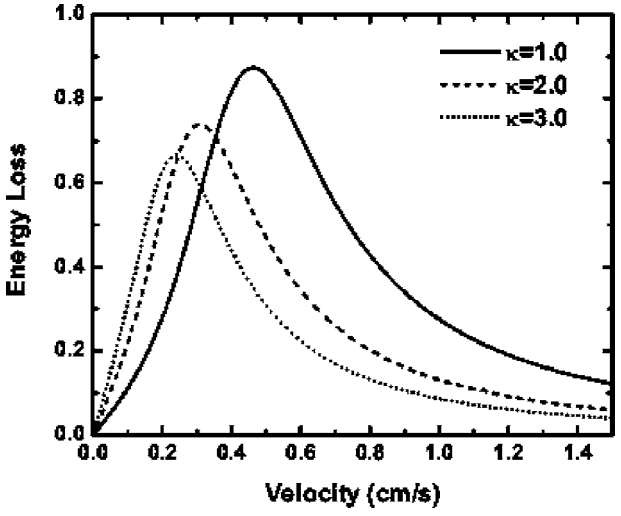

FIG. 11. The normalized energy loss, $S\lambda_D/T_e$, of the projectile charge versus its velocity in a dusty plasma, based on the QLCA description, for different screening constants: $\kappa=1$, $\kappa=2$, and $\kappa=3$. Here, the coupling constant $\Gamma=1000$, the discharge pressure $p=10$ Pa, and the height of the particle $h=2\lambda_D$ are kept fixed.

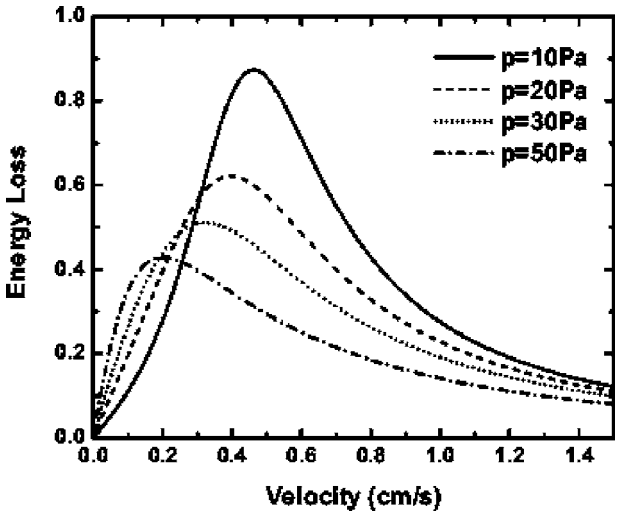

FIG. 12. The normalized energy loss, $S\lambda_D/T_e$, of the projectile charge versus its velocity in a dusty plasma, based on the QLCA description, for different discharge pressures: $p=10$ Pa, 20 Pa, 30 Pa, and 50 Pa. Here, the coupling constant $\Gamma=1000$, the screening constant $\kappa=1$, and the height of the particle $h=2\lambda_D$ are kept fixed.

Figure 4 shows the perturbed density σ_{d1} in the Mach-cone region for $\kappa=1$, 2, and 3, with $\Gamma=1000$, $v=1$ cm/s, and $p=10$ Pa kept fixed. One can see that the amplitude of Mach cones increases, and the wake effect becomes more pronounced, with increasing κ. Figure 5 shows the profile of the velocity field $\mathbf{u}_{d1}$ in the Mach cone region for the same parameters as in Fig. 4, indicating that the opening angle shrinks as κ increases. Noting that $\kappa=a/\lambda_D$, one can conclude that Mach cones with higher amplitudes, narrower opening angles, and more pronounced wake fields can be achieved by increasing the average interparticle distance a.

Figures 6 and 7 further show the influence of the projectile particle speed on the Mach-cone structure for $v=0.5$ cm/s, 1 cm/s, and 1.5 cm/s, with the discharge pressure $p=10$ Pa, $\Gamma=1000$, and $\kappa=1$ kept fixed. It is clear from these figures that both the magnitudes and the opening angles of Mach cones decrease with increasing speed.

In order to illustrate the damping effects due to the neutral friction, we next vary the discharge pressure. Figures 8 and 9 display the perturbed density and the fluid velocity in the Mach-cone region, respectively, for the pressures $p=5$ Pa, 10 Pa, and 15 Pa, with $v=1$ cm/s, $\Gamma=1000$ and $\kappa=1$ kept fixed. The main influence of increasing pressure is seen to dampen the wake-field oscillations, with a slight decrease in the magnitude of Mach cones. This has an apparent effect of reducing the number of Mach cones down to two or even one, which is similar to our earlier results achieved by means of the RPA description [38]. It has been also found earlier that the discharge pressure plays a similar role in the laser-excited Mach cones in dusty plasmas [23].

III. ENERGY LOSS

Energy loss of the projectile charge per unit path length, or its stopping power, is an important quantity

for describing the interactions of external probe particles with dusty plasmas. For charged particles moving in weakly coupled 3D dusty plasmas, the energy loss is well understood on the basis of the linear Vlasov-Poisson theory [26–29]. For a strongly coupled 2D dusty plasma, the stopping power S can be calculated from the QLCA results in conjunction with Poisson equation, by using the definition

$$S(v) = eZ_t \left. \frac{\partial \Phi_{ind}}{\partial x} \right|_{z=h,\mathbf{r}=\mathbf{v}t}, \tag{16}$$

where $\Phi_{ind}=\Phi-\Phi_{ext}$ is the induced potential in the system. Full spatial dependence of the total electrostatic potential, $\Phi(\mathbf{R},t)$, can be determined from the 3D Poisson equation,

$$\nabla^2\Phi(\mathbf{R},t) = -4\pi e[n_i(\mathbf{R},t) - n_e(\mathbf{R},t) - Z_d\sigma_d(\mathbf{r},t)\delta(z) + \rho_{ext}(\mathbf{R},t)], \tag{17}$$

with $\boldsymbol{\nabla}=\boldsymbol{\nabla}_{\mathbf{r}}+\hat{\mathbf{z}}(\partial/\partial z)$ and $\rho_{ext}(\mathbf{R},t)=-Z_t e\,\delta(\mathbf{r}-\mathbf{v}\mathbf{t})\delta(z-h)$ being the projectile charge density. The electron and the ion volume densities are given by Boltzmann relations, $n_e=n_0\exp(e\Phi/T_e)$ and $n_i=n_0\exp(-e\Phi/T_i)$, owing to the fact that the disturbances in plasma caused by the motion of massive dust particles are so slow that both the electrons and the ions have enough time to reach their respective local equilibria, with $T_{i(e)}$ being the ion (electron) temperature.

Considering Φ_{ext} a small disturbance, we linearize Eq. (17) by assuming $\Phi(\mathbf{R},t)=\Phi_0(z)+\Phi_1(\mathbf{R},t)$, $\sigma_d(\mathbf{r},t)=\sigma_{d0}+\sigma_{d1}(\mathbf{r},t)$, $n_e(\mathbf{R},t)=n_{e0}(z)+n_0(e/T_e)\Phi_1(\mathbf{R},t)$, and $n_i(\mathbf{R},t)=n_{i0}(z)-n_0(e/T_i)\Phi_1(\mathbf{R},t)$, where $n_{e0}(z)$, $n_{i0}(z)$, and $\Phi_0(z)$ are the unperturbed values of the electron density, ion density, and the potential in the absence of the projectile charge [23]. Using 2D Fourier transform in the (x,y) plane we obtain the equation

$$\frac{\partial^2}{\partial z^2}\Phi_1(\mathbf{k},z,\omega) - (k^2\lambda_D^2+1)\lambda_D^{-2}\Phi_1(\mathbf{k},z,\omega) = 4\pi e Z_d\sigma_{d1}(\mathbf{k},\omega)\delta(z) + 8\pi e Z_t\delta(\omega-\mathbf{k}\cdot\mathbf{v})\delta(z-h), \tag{18}$$

which is easily solved by using the natural boundary conditions for Φ_1 at $z=0$ (continuity of Φ_1 and $\Phi_1'(0+)-\Phi_1'(0-)=4\pi e Z_d\sigma_{d1}$), so that the induced potential, $\Phi_{ind}(\mathbf{R},t)=\Phi_1(\mathbf{R},t)-\Phi_{ext}(\mathbf{R},t)$, can be expressed as

$$\Phi_{ind}(\mathbf{r},z,t) = \frac{eZ_t\omega_{pd}^2\lambda_D}{2\pi}\int d^2\mathbf{k}\frac{(k\lambda_D)^2\exp\left(-\frac{|z|+h}{\lambda_D}\sqrt{1+(k\lambda_D)^2}+i\mathbf{k}\cdot(\mathbf{r}-\mathbf{v}t)\right)}{[1+(k\lambda_D)^2]\cdot H_L(k,\mathbf{k}\cdot\mathbf{v})}. \tag{19}$$

Finally, using Eqs. (16) and (19), the stopping power becomes

$$S(v) = \frac{\omega_{pd}^2(eZ_t)^2\lambda_D}{2\pi v}\int d^2\mathbf{k}\frac{(k\lambda_D)^2}{1+(k\lambda_D)^2}\frac{\gamma\omega^2\exp\left[-\frac{2h}{\lambda_D}\sqrt{1+(k\lambda_D)^2}\right]}{\{\omega^2-\omega_0^2(k)[1+D_L(k)]\}^2+(\gamma\omega)^2}, \tag{20}$$

where $\omega=\mathbf{k}\cdot\mathbf{v}$.

We now use the same parameters for the bulk plasma and the dust layer as in the preceding section to calculate the energy loss. Figure 10 shows the influences of the coupling constant Γ on the energy loss $S(v)$ (normalized by T_e/λ_D), for both the QLCA [Fig. 10(a)] and the RPA [Fig. 10(b)] models. Each case shown in Fig. 10 displays a characteristic curve with a peak, or with a maximum rate of energy loss, occurring for certain speed of the projectile charge. It is clear that both the peak heights and their positions in the $S(v)$ curves increase with Γ for both models. Furthermore, by comparing Figs. 10(a) and 10(b), it appears that the peaks in $S(v)$ take higher values and occur at lower speeds when the correlation effects of the dust layer are included. In fact, the two sets of curves from QLCA and RPA models are seen to almost coincide at high speeds for all Γ values displayed, but the low-speed energy loss is suppressed in the RPA model due to the lack of interparticle correlations. In Figs. 11 and 12, we show respectively the influences of the screening parameter κ and the discharge pressure p on the normalized energy loss $S(v)$ in the QLCA model. It is seen that, when both κ and p increase, the energy losses at high speeds are suppressed and the low-speed losses increased, effectively giving rise to lowering of the peak values and their shifting to lower speeds.

IV. CONCLUDING REMARKS

This work presents a theoretical description of the interactions of moving charged particles with 2D strongly coupled dusty plasmas, which takes into account the correlation between the dust particles and the damping effects due to the dust collisions with neutral plasma particles. Numerical results for the perturbed density and velocity fields in the dust layer exhibit Mach cones with the characteristic oscillatory wake patterns, which are in good qualitative agreement with the experimental [16,17] and theoretical results [20]. Special attention in our analysis is paid to the dependencies of the Mach-cone structure on the coupling parameter Γ, the screening parameter κ, and the discharge pressure p. In com-

parison with the random-phase approximation results, the strong coupling effects are found to exert substantial influences on the structure of Mach cones.

We also study the energy loss of an external charged projectile moving over the dust layer based on the QLCA-Poisson theory. Numerical results show strong influences of the coupling constant, the screening constant, and the discharge pressure on the projectile energy loss. In particular, it is found that the correlation effects of the dust particles enhance the energy loss of the projectile particle at lower speeds. Quantitatively, it is found that the slowing down of the projectile particle amounts to deaccelerations in the range of -0.1 to -1 cm/s^2 for the parameters used, which can be experimentally measured. It should be noted that the competing processes of acceleration of external charged particles remains a fascinating phenomenon [16,17,37], which we currently investigate in extensions of our simulation method taking into account the acceleration mechanism suggested by Schweigert *et al.* [37], on the basis of instability arising from asymmetric interaction between a particle in the dust layer and the projectile particle. Finally, future amendments to our model will take into account the effects of motion on the charge distribution on the projectile particle.

ACKNOWLEDGMENTS

This work was supported by the Research Fund for the Doctoral Program of Higher Education of China (Grant No. 20050141001) (Y.N.W.). Supports from NSERC and PREA are also acknowledged (Z.L.M.).

[1] H. Ikezi, Phys. Fluids **29**, 1764 (1986).
[2] Y. Hayashi and K. Tachibana, Jpn. J. Appl. Phys., Part 2 **33**, L804 (1994).
[3] J. H. Chu and L. I., Phys. Rev. Lett. **72**, 4009 (1994).
[4] H. Thomas, G. E. Morfill, V. Demmel, J. Goree, B. Feuerbacher, and D. Mohlmann, Phys. Rev. Lett. **73**, 652 (1994).
[5] A. Melzer, T. Trottenberg, and A. Piel, Phys. Lett. A **191**, 301 (1994).
[6] F. M. Peeters and X. Wu, Phys. Rev. A **35**, 3109 (1987).
[7] Y. Wang, C. Jin, S. Han, B. Cheng, and D. Zhang, Jpn. J. Appl. Phys., Part 1 **43**, 1666 (2004).
[8] S. Nunomura, J. Goree, S. Hu, X. Wang, A. Bhattacharjee, and K. Avinash, Phys. Rev. Lett. **89**, 035001 (2002).
[9] S. Zhdanov, S. Nunomura, D. Samsonov, and G. Morfill, Phys. Rev. E **68**, 035401(R) (2003).
[10] X. Wang, A. Bhattacharjee, and S. Hu, Phys. Rev. Lett. **86**, 2569 (2001).
[11] S. Nunomura, J. Goree, S. Hu, X. Wang, and A. Bhattacharjee, Phys. Rev. E **65**, 066402 (2002).
[12] N. Rao, P. Shukla, and M. Yu, Planet. Space Sci. **38**, 543 (1990).
[13] A. Barkan, R. Merlino, and N. D'Angelo, Phys. Plasmas **2**, 3563 (1995).
[14] M. Rosenberg and G. Kalman, Phys. Rev. E **56**, 7166 (1997).
[15] O. Havnes, T. Aslaksen, T. W. Hartquist, F. Li, F. Melandsø, G. E. Morfill, and T. Nitter, J. Geophys. Res. **100**, 1731 (1995).
[16] D. Samsonov, J. Goree, Z. W. Ma, A. Bhattacharjee, H. M. Thomas, and G. E. Morfill, Phys. Rev. Lett. **83**, 3649 (1999).
[17] D. Samsonov, J. Goree, H. M. Thomas, and G. E. Morfill, Phys. Rev. E **61**, 5557 (2000).
[18] A. Melzer, S. Nunomura, D. Samsonov, Z. W. Ma, and J. Goree, Phys. Rev. E **62**, 4162 (2000).
[19] V. Nosenko, J. Goree, Z. W. Ma, and A. Piel, Phys. Rev. Lett. **88**, 135001 (2002).
[20] D. Dubin, Phys. Plasmas **7**, 3895 (2000).
[21] P. K. Shukla, A. A. Mamun, and R. Bingham, JETP Lett. **78**, 99 (2003).
[22] P. K. Shukla and A. A. Mamun, Phys. Lett. A **315**, 258 (2003).
[23] L. J. Hou, Y. N. Wang, and Z. L. Mišković, Phys. Rev. E **70**, 056406 (2004).
[24] A. A. Mamun, P. K. Shukla, and G. E. Morfill, Phys. Rev. Lett. **92**, 095005 (2004).
[25] Z. W. Ma and A. Bhattacharjee, Phys. Plasmas **9**, 3349 (2002).
[26] M. H. Nasim, A. M. Mirza, M. S. Qaisar, G. Murtaza, and P. K. Shukla, Phys. Plasmas **5**, 3581 (1998).
[27] M. H. Nasim, M. S. Qaisar, A. M. Mirza, G. Murtaza, and P. K. Shukla, Phys. Plasmas **7**, 762 (2000).
[28] S. Ali, M. H. Nasim, and G. Murtaza, Phys. Plasmas **10**, 4207 (2003).
[29] A. M. Mirza, M. A. Sarwar, and M. S. Qaisar, Phys. Plasmas **10**, 4253 (2003).
[30] G. Kalman and K. I. Golden, Phys. Rev. A **41**, 5516 (1990).
[31] K. I. Golden, G. Kalman, and P. Wyns, Phys. Rev. A **41**, 6940 (1990).
[32] K. I. Golden and G. J. Kalman, Phys. Plasmas **7**, 14 (2000).
[33] G. Kalman, M. Rosenberg, and H. E. DeWitt, Phys. Rev. Lett. **84**, 6030 (2000).
[34] G. J. Kalman, P. Hartmann, Z. Donkó, and M. Rosenberg, Phys. Rev. Lett. **92**, 065001 (2004).
[35] P. Epstein, Phys. Rev. **23**, 710 (1924).
[36] X. H. Zheng and J. C. Earnshaw, Phys. Rev. Lett. **75**, 4214 (1995).
[37] V. A. Schweigert, I. V. Schweigert, V. Nosenko, and J. Goree, Phys. Plasmas **9**, 4465 (2002).
[38] K. Jiang, L. J. Hou, and Y. N. Wang, Chin. Phys. Lett. **22**, 1713 (2005).